Dielectric-modulated biosensing with ultrahigh-frequency-operated graphene field-effect transistors

Zhang, X.; Liu, T.; Boyle, A.L.; Bahreman, A.; Jing, Q.; Xue, H.; ... ; Fu, W.

ADVANCED MATERIALS
www.advmat.de

Dielectric-Modulated Biosensing with Ultrahigh-Frequency-Operated Graphene Field-Effect Transistors

Xiaoyan Zhang, Tingxian Liu, Aimee Boyle, Azadeh Bahreman, Lei Bao, Qiushi Jing, Honglei Xue, Roxanne Kieltyka, Alexander Kros, Grégory F. Schneider,* and Wangyang Fu**

Owing to their excellent electrical properties and chemical stability, graphene field-effect transistors (Gr-FET) are extensively studied for biosensing applications. However, hinging on surface interactions of charged biomolecules, the sensitivity of Gr-FET is hampered by ionic screening under physiological conditions with high salt concentrations up to frequencies as high as MHz. Here, an electrolyte-gated Gr-FET in reflectometry mode at ultrahigh frequencies (UHF, around 2 GHz), where the ionic screening is fully cancelled and the dielectric sensitivity of the device allows the Gr-FET to directly function in high-salt solutions, is configured. Strikingly, by simultaneous characterization using electrolyte gating and UHF reflectometry, the developed graphene biosensors offer unprecedented capability for real-time monitoring of dielectric-specified biomolecular/cell interactions/activities, with superior limit of detection compared to that of previously reported nanoscale high-frequency sensors. These achievements highlight the unique potential of ultrahigh-frequency operation for unblocking the true potential of graphene biosensors for point-of-care diagnostic.

1. Introduction

Driven by the prospect of integrating biodetection capabilities into existing semiconductor technology, researchers have been actively pursuing the brilliant idea of ion-sensitive field-effect transistors (ISFETs) based on charge sensing mechanism,[1–12] with proof-of-principle demonstrations regarding the detection of biotin–streptavidin binding, antibody–antigen interaction, DNA hybridization, cell activity, and so on. Unfortunately, the sensitivity of the ISFETs is greatly compromised because of the chemical instability of conventional semiconducting materials (Si, Ge, GaAs, etc.),[6–8,11] where a relatively thick passivation/insulating oxide layer is needed and inevitably leads to a weak coupling. In this regard, by serving as both the sensor channel and the surface, chemically inert graphene with excellent electrical properties, enables ultimate sensitivity towards single or few molecular detections.[13,14] Yet, the target biomolecules binding on receptor biomolecules of several nanometers away from the graphene surface (and ISFET in general), are unable to induce a notable field effect due to electrical screening by counterions in high-salt solutions at direct current or low frequencies, representing a major drawback for biosensing under physiological conditions. To mitigate the fundamental ionic screening effect, high-frequency single-walled carbon nanotube heterodyne sensors have been used.[15] Nevertheless, the fact that the transconductance-dependent heterodyne output signal could be modeled as a result of an effective double-layer-capacitance coupling between the electrolyte gate and the nanotube channel up to 10 MHz, suggests that ionic screening is still relevant at such high frequencies.[15,16]

On the other hand, owing to the high carrier mobility and saturation velocity,[13] graphene FETs (Gr-FETs) have received worldwide interests in the domain of high-frequency electronics, providing an ideal platform for real-time sensing applications under physiological conditions by overcoming the ionic screening of movable ions.[17–19] Importantly, in contrast to conventional metal-based interdigitated capacitors or transmission line with invariant electrical properties, the type of carriers as well as the carrier density of Gr-FETs can be effectively tuned using electrolyte gating and/or upon biomolecular adsorption, representing a significant advantage for the development and optimization of advanced high-frequency biosensors.

Here, to fully overcome the ionic screening effect in high-salt solutions, we configured electrolyte-gated Gr-FET in reflectometry mode at ultrahigh frequencies (UHF, around 2 GHz) and achieved orders-of-magnitude lower limits of detection (LOD) compared to those of previously reported metal or nanomaterial-based high-frequency sensors. Strikingly, by simultaneously characterized using electrolyte gating and UHF reflectometry, we were able to unmix/differentiate the correlated field-effect and UHF sensing response, thus offering unprecedented capability for real-time monitoring of dielectric-specified biomolecular/cell interactions/activities. These achievements

X. Zhang, L. Bao, Q. Jing, H. Xue, W. Fu
School of Materials Science and Engineering
Tsinghua University
No.1 Tsinghua Yuan, Haidian District, Beijing 100084, China
E-mail: xyzhang@iccas.ac.cn; fwy2018@mail.tsinghua.edu.cn
X. Zhang, T. Liu, A. Boyle, A. Bahreman, R. Kieltyka, A. Kros, G. F. Schneider
Faculty of Science
Leiden Institute of Chemistry
Leiden University
Einsteinweg 55, Leiden 2333CC, The Netherlands
E-mail: g.f.schneider@chem.leidenuniv.nl
The ORCID identification number(s) for the author(s) of this article can be found under https://doi.org/10.1002/adma.202106666.

DOI: 10.1002/adma.202106666

highlight the unique potential of ultrahigh-frequency operation to unblock the true potential of graphene biosensors for point-of-care (POC) diagnostics, where directly functioning in physiological conditions with high salt concentrations is desired.

2. Results and Discussion

2.1. Ultrahigh-Frequency-Operated Gr-FET Sensor Fabrication and Sensing Principle

Starting with high-quality single-crystal chemical vapor deposition (CVD) graphene (Figure S1, Supporting Information), we patterned and metalized micrometer-sized graphene ribbon via standard electron beam lithography (EBL). For liquid handling, we applied a microfluidic channel (SU-8 photoresist layer of 1 µm thickness) placed across the graphene ribbon (upper panel, **Figure 1**A and Figure S1, Supporting Information). Together with the electrolyte solution in the microfluidic channel, a commercial Red Rod reference electrode was adopted as the electrolyte gate. To optimize the sensor design, we constructed a gold electrode on the lateral side of the graphene ribbon (with a gap of 200 nm unless stated otherwise, lower panel, Figure 1A and Figure S1, Supporting Information). Along with the nanoscale gap, the microfluidic channel placed across the graphene ribbon not only prevents leakage current from the metal contacts, but also limits possible loss in sensitivity due to the radio frequency (RF) field spreading into the bulky liquid environment. That is, the evanescent nature of the electromagnetic fields combined with the abrupt changes in the dielectric properties at the interface (and particularly at the gap), result in a highly localized and concentrated electromagnetic field (Figure S2, Supporting Information). Therefore, biomolecules that bind at the graphene edge/gap are expected to significantly influence the evanescent electromagnetic fields concentrated at the ribbon/aqueous interface.

Prior to the real-time sensing, the graphene ribbon sensor was mounted on a RF box (Figure 1A and Figure S3, see also the Experimental Section), whose reflection coefficient *S*11 was characterized using RF reflectometry. As shown in Figure 1B, the resonance frequency decreased from 1.935 GHz (black curve) to 1.83 GHz (red curve) after a connection to the

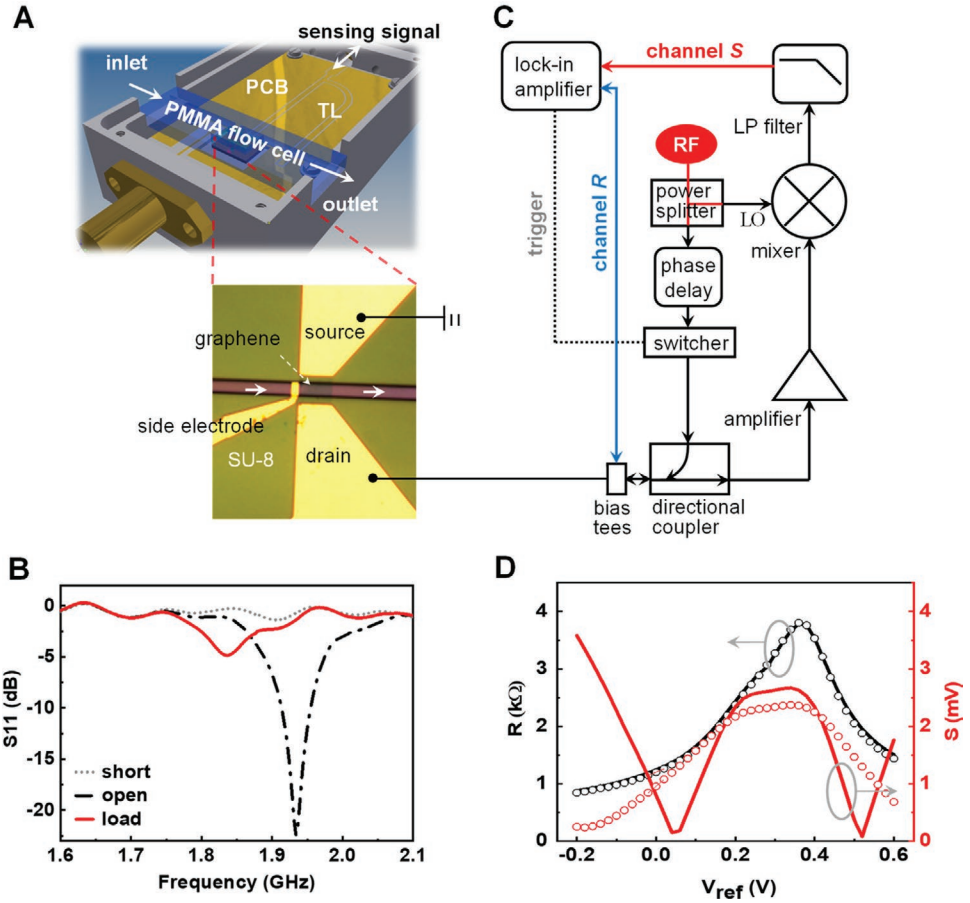

Figure 1. A) Schematic of the graphene UHF device. The lower panel shows an optical image of the fabricated Gr-FET with a liquid channel (indicated by the two arrows in white) made of SU-8 photoresist. The graphene chip is mounted and wire-bonded on a printed circuit board (PCB, see Figure S3, Supporting Information), after which the transparent flow cell (PMMA) is assembled on top of the graphene chip in the RF box (upper panel). This RF box is connected to the experimental setup to perform the reflectometry measurements at UHF of ≈2 GHz. B) UHF reflectometry measurements. C) The schematics of the UHF biological graphene sensor setup. Both the graphene resistance signal (*R*) and the UHF signal (*S*) can be sampled at the same time. D) Field-effect- or electrolyte-gate-induced sheet resistance *R* and UHF capacitive signal *S* variations. Lines are measured at 1.92 GHz and dots are measured at 1.82 GHz, respectively.

poly(methyl methacrylate) (PMMA) flow cell filled with electrolyte, mainly due to the additional capacitance of water adsorption on the sensor surface. We note here that the chosen UHF of around 2 GHz is also optimized for accurate biological detection, as biomolecules/cells and water exhibit distinct contrasts in permittivity and the sensing signal can be primarily and preferentially related to changes in capacitance.[20]

Importantly, in contrast to conventional metal-based UHF sensors, graphene UHF sensors could additionally, even simultaneously, be characterized by using electrolyte gating for comparison. Figure 1C illustrates the corresponding schematic diagram of our home-made biological sensor setup (Figure S4, Supporting Information, see also the Experimental Section), where we sampled both the UHF interferometry sensing signal S (in red) and the graphene resistance R (in blue) using a two-channel lock-in amplifier, yielding UHF sensing and classical field-effect sensing, respectively. Figure 1D depicts the electrolyte gate dependent measurements. That is, the electrostatic coupling between the graphene channel and the reference electrode via the electrolyte leads to a gate-induced sheet resistance variation, from which we deduced a relatively high field-effect carrier mobility of 2100 $cm^2\ V^{-1}\ s^{-1}$. We also observed an electrolyte-gate modulated UHF signal S depending on the choice of operation frequencies (Figure 1D, red line: 1.92 GHz, red dots: 1.82 GHz). Interestingly, depending on the electron or hole operation region, the UHF signal S exhibits a different value even at the same graphene resistance R. We ascribe such electrolyte-gate dependent behavior of the UHF signal S to the asymmetry of electron and hole carriers in doped graphene samples, which leads to asymmetric variations in the quantum capacitance of graphene.[21] Thus, the gate-induced resistance, which is not obtainable with metal materials, as well as the tunable electrical properties of graphene at UHF, are of key importance for the development and optimization of dielectric-modulated Gr-FET biosensors for directly measuring in physiological conditions.

2.2. Dielectric-Modulated Detection of Charged or Neutral Biomolecules

To explore the scope of graphene UHF sensors for dielectric-modulated detection, we investigated the well-characterized biotin–streptavidin binding and the interaction between two complementary peptides forming heterodimeric coiled-coil complex as model systems. With a binding constant of around $10^{14}\ M^{-1}$, the biotin–streptavidin system is the strongest and best known natural noncovalent pair between a protein (60 kDa, almost no net charge) and a small molecule ligand. For coiled-coil formation, we studied the well-characterized heterodimeric peptide pair dubbed E/K.[22] At neutral pH, peptide E (i.e., $(EIAALEK)_3$) is negatively charged while peptide K (i.e., $(KIAALKE)_3$) is positively charged and coiled-coil formation is driven by a combination of hydrophobic and electrostatic interactions. Upon incorporation into liposomal membranes, coiled-coil formation between lipidated derivatives of peptides E/K drives membrane fusion,[23,24] mimicking natural coiled-coil mediated fusion processes such as exocytosis and neurotransmission.[25]

Considering that precise control of the UHF biosensor interfacing is critical for selective detection of biomolecules, we first noncovalently labeled graphene using biotin molecules (or peptide E, not shown here) functionalized with pyrene–PEG linker groups (**Figure 2**A) at 10×10^{-6} M concentration in phosphate buffer saline (PBS) solution. Without losing the generality, here we deliberately adopted the 4 nm-long PEG_{10} block to demonstrate that under UHF, one can manage to realize dielectric-modulated detection of biomolecules more than 4 nm away from the sensing surface far beyond the Debye screening length of 0.7 nm. In Figure 2B, abrupt changes of both UHF (S, in red) and classical resistance (R, in black) signal can be traced upon introduction of the linker groups, confirming the successful functionalization of graphene by pyrene-linked biotin. The increased R of graphene upon pyrene adsorption, indicates either the collision of carriers by additional scattering centers or the change of carrier density caused by charge transfer. To fully understand the sensing mechanism, in Figure S5A/B (Supporting Information), we evaluated: i) the shift of the Dirac point or gate voltage ΔV_{ref}, ii) the change of the transconductance Δg_m, and iii) the change of the carrier mobility μ,[26] based on the transfer characteristics of another Gr-FET device upon pyrene–PEG_{10}–biotin decorating. It is found that the Dirac point shifted –100 mV upon the adsorption of pyrene–PEG_{10}–biotin due to charge transfer. Interestingly, after functionalization the transconductance and the carrier mobility generally decreases in the electron region, but retains in the hole region (please see the Supporting Information for more detailed discussions), suggesting that pyrene surface functionalization is conducive to electron scattering rather than hole scattering. In fact, this finding that except for the Dirac point shift, the addition of aromatic molecules preserved both the transconductance and the carrier mobility of the Gr-FET to a large extent, is in good agreement with previous experimental results.[26] We note here that adding streptavidin or K peptide beyond the Debye screening length in buffer solution with high ionic strength, exhibits no (systematic) sensing signal. On the other hand, the UHF signal S (Figure 2B, in red) is a function of both the electrical properties of graphene and the local capacitance variations due to attachment of pyrene-linked biotin. By deducing the variations of S originated from the changes in the graphene carrier concentration in the hole region with preserved carrier mobility, we are capable of deducing a dielectric-modulated UHF signal (Figure 2B, in pink), which gives the changes in S due to local capacitance variations upon pyrene-linked biotin adsorption.

For dielectric-modulated UHF sensing, we injected streptavidin at 1×10^{-9} and 1×10^{-6} M concentrations as indicated by the black and the red arrows, respectively, in Figure 2C. The streptavidin strongly binds to the biotin molecules adsorbed on graphene from a distance of 4 nm (estimated based on the length of the pyrene–PEG_{10} linker group), and induces a strong increase in the UHF sensing signal ΔS as recorded by the UHF graphene sensor at a streptavidin concentration as low as 1×10^{-9} M. In contrast, the classical Gr-FET sensing failed to detect a positive signal as indicated by the continuous flat baseline in black (upon 1×10^{-9} M streptavidin injection). Studies on pyrene–PEG_{10}–biotin and/or pyrene–PEG_{12}–E/K surface functionalization demonstrated that there are sections or area of graphene not coated with pyrene–PEG_{10}–biotin

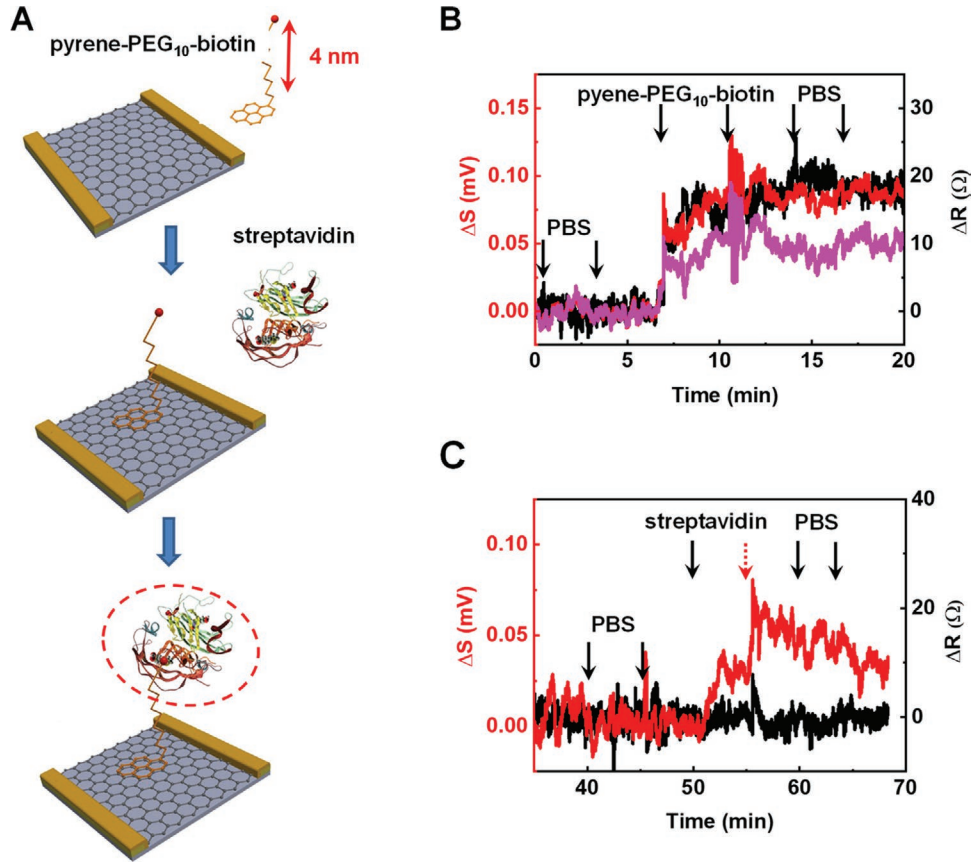

Figure 2. A) Schematics of biotin functionalization and streptavidin detection. The graphene surface of the sensor is first functionalized with biotin (represented by the red dot) conjugated to pyrene via a relatively long PEG_{10} chain (≈4 nm). Streptavidin was introduced and strongly binds to the biotin molecules bound to graphene. B) The pyrene anchors on the graphene surface via π–π interactions as shown by the sudden drop in both the conventional resistance (the black line) and UHF sensing signals (the red line). The pink line represents a dielectric-modulated UHF signal after deducing the variations of the UHF sensing signal S originated from the changes in the graphene carrier concentration. C) Upon introduction, streptavidin binds to biotin as revealed by a change in dielectric-modulated UHF sensing signal while the conventional Gr-FET sensing signal is unable to detect this binding event.

and/or pyrene–PEG_{12}–E/K. Further surface functionalization using Tween-20 can block and passivate these areas for nonspecific adsorption. We also characterized the Gr-FET before and after coating linkers and target molecular sensing by using atomic force microscopy (AFM) (Figure S6, Supporting Information) and quartz crystal microbalance with dissipation (QCM-D, Figure S7, Supporting Information), to evaluate the functionalization of pyrene–PEG_{10}–biotin and passivation of Tween-20, leading to the conclusion that the adsorptions are stable and reproducible. We note here that we cannot rule out multiple staking or uneven distribution of these polymers. Nevertheless, multiple staking of weak coupling is intended to be rinsed away by sufficient buffer solution. In a separated measurement under 100 times diluted PBS buffer solutions (with Debye screening length of 7 nm, and thus not ionic screening effect), we performed the calibration by introducing streptavidin at 100×10^{-9} M concentrations (Figure S8A, Supporting Information). Repeated adding of 100×10^{-9} M streptavidin led to no change of sensing response after the first signal, the saturation of which approves the picture of biotin-limited detection, due to the extremely high association constant of streptavidin onto biotin (10^{14} M^{-1}). This additional experiment is in good agreement with the results presented in Figure 2C, where the nonreversible binding of streptavidin on biotin causes an ambiguous sensing response at 1×10^{-9} M but not at 1×10^{-6} M after rinsing in the continuous measurements. We ascribed the UHF sensing response at 1×10^{-6} M (which is equal to ≈1 streptavidin molecule per 100 nm × 100 nm × 100 nm volume) to the concentrated streptavidin solutions with reduced dielectric constant. The sensing of 1×10^{-9} M is biotin-limited, as any nonspecific adsorption is blocked by using Tween-20 passivation. Given the equilibrium disassociation constant K_D of 10^{-14} M and association rate constant k_1 of 10^8 M^{-1} s^{-1} (with disassociation rate constant k_{-1} on the order of 10^{-6} s^{-1}, $K_D = k_{-1}/k_1$) of the biotin-streptavidin system,[27] we reasonably assume that all biotins are occupied by streptavidin at 1×10^{-9} M within our measurement duration of several minutes. We note here that this highly sensitive detection of streptavidin is achieved under a rather neutral pH = 8.1, where streptavidin has almost no net charge. Compared to the estimated limit of detection (LOD, 2×10^{-6} M) of the previously reported carbon nanotube RF mixers[15] or conventional dielectric-modulated silicon field-effect biosensors (LOD, $\approx 3 \times 10^{-3}$ M),[7,28] we ascribe the sensitive detection of streptavidin with orders-of-magnitude

improved LOD (1×10^{-9} M) to the adoption of impedance matching circuits, and particularly, to the UHF operation frequencies with nanogap configuration, where the ionic screening effect is fully cancelled and distinct differences in the dielectric constant between the biomolecules and the water dipoles are amplified.

For order-of-magnitude estimation, based on Equation 1 (see the Experimental Section), $\Delta S = 30$ μV (Figure 2C) corresponds to a capacitance change of $\Delta C = 35$ aF. Theoretically, the change is proportional to the nonuniform electric field concentrated at the graphene edge $|E_{edge}|^2$, which can be deduced by using COSMOL MULTIPHYSICS.[20] Assuming a radius of 4 nm and a dielectric constant of 5 for the streptavidin molecule, we may ascribe the observed capacitance change to a dense adsorption of the biomolecules along the graphene edge (≈1 per 50 nm, which is in agreement with our AFM results, see Figure S6, Supporting Information). In principle, even an individual binding event (streptavidin onto biotin receptor) could be identified if one can introduce a nanofluidic channel to further constraint the electric field and reduce further the electrical noise.

In another experiment to validate our sensing approach, pyrene–PEG_{12}-linked E peptide was absorbed onto graphene and measured the response of the functionalized UHF graphene sensor to K peptide binding via coiled-coil formation in real time (**Figure 3**A). The abrupt decrease in the capacitance signal sampled by the time-resolved interferometer measurement confirms the adsorption of pyrene–PEG_{12}–E on the Gr-FET (Figure S9, Supporting Information, see also Figure S5 Supporting Information, for more related results and discussions). The monitored dielectric-modulated UHF sensing signal S increases upon 1×10^{-9} M K peptide introduction (Figure 3B). In a separated measurement (Figure S10, Supporting Information), we tested the sensing response of the device to K peptide at 1×10^{-9} M concentration and no resistance change can be detected after equilibration. The abrupt peaks can be ascribed to the injection of test solutions. Its magnitude is 50 μV; the background root mean square (RMS) noise is 10 μV, giving a signal-to-noise ratio (SNR) of 5. Upon further rinsing with PBS, the sensing signal shifts back to its original level, suggesting reversible binding dynamics, which is reasonable given the dissociation constant of this coiled-coil pair is in the $\times 10^{-9}$ M range.[29] The reproduced sensing signal in Figure 3B further suggests that the E/K coiled-coil can form at 1×10^{-9} M concentration reproducibly. We also performed the concentration-dependent sensing experiments of E/K by introducing E peptide at 10×10^{-9} M, 100×10^{-9} M, and 1×10^{-6} M concentrations (Figure S8B, Supporting Information). The gradually increased resistance sensing signal can be calibrated for deducing the association constant of 1.4×10^{8} M^{-1} for E/K coiled-coil interaction (Figure S8B, Supporting Information), a modest value explains the observed reversible binding of E peptides on K peptides and is in consistent with previous reports.[30]

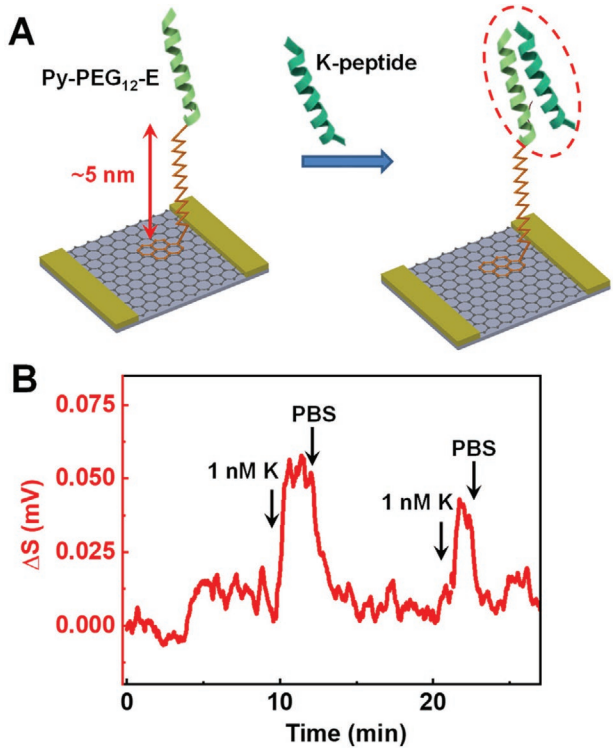

Figure 3. A) Schematics of a pyrene linker group was attached to peptide E (i.e., $(EIAALEK)_3$) with a relatively long PEG_{12} chain (≈5 nm). B) Dielectric-modulated detection of pyrene–PEG_{12}–E interacts with the introduced peptide K (i.e., $(KIAALKE)_3$) via a coiled-coil interaction by the UHF graphene sensor.

2.3. Dielectric-Modulated Detection of Cell Action of Cardiomyocytes

We extend the UHF measurement to record the action of electrogenic cells, i.e., cardiomyocytes cultured on the entire graphene chip with a density of ≈5000 cells mm^{-2} (see the Experimental Section for details). The inset of **Figure 4**A gives the scheme of such a cardiomyocyte seeded on graphene (see also Movie S1 and Figure S7, Supporting Information, for electrogenic cells exhibiting healthy growth). In Figure 4A, we simultaneously recorded the time traces of both the conventional Gr-FET sensing signal (ΔR) and the UHF sensing signal (ΔS). We note here that we have calibrated the ΔS using the ΔR to exclude contributions from graphene carrier density due to action potential of the cell membrane. Thus, the calibrated dielectric-modulated UHF signals represent cell contractility at a rate over 7 beat per minute (bpm) in accordance with a previous report[29] with an amplitude of 85 ± 2 μV, which corresponds to 20% contraction for a cardiomyocyte cell with a dielectric constant of 50 and about 100 μm long and 10 μm in diameter.[20] Remarkably, in contrast to conventional Gr-FET detection of action potential, we are capable of probing deeply into the solution and cell body by fully overcoming the ionic screening effect using UHF measurement. This provides a unique opportunity to detect changes in the contractility of the cell, which is crucial for certain drug screening application, e.g., in case of blebbistatin, an inhibitor of myosin II can impair the contractile machinery of the cardiomyocytes, while not interfere with ion channel function.

Last but not least, to provide a comprehensive understanding of the high-frequency sensing mechanism, we investigated the distance dependency of the UHF biological sensor. We

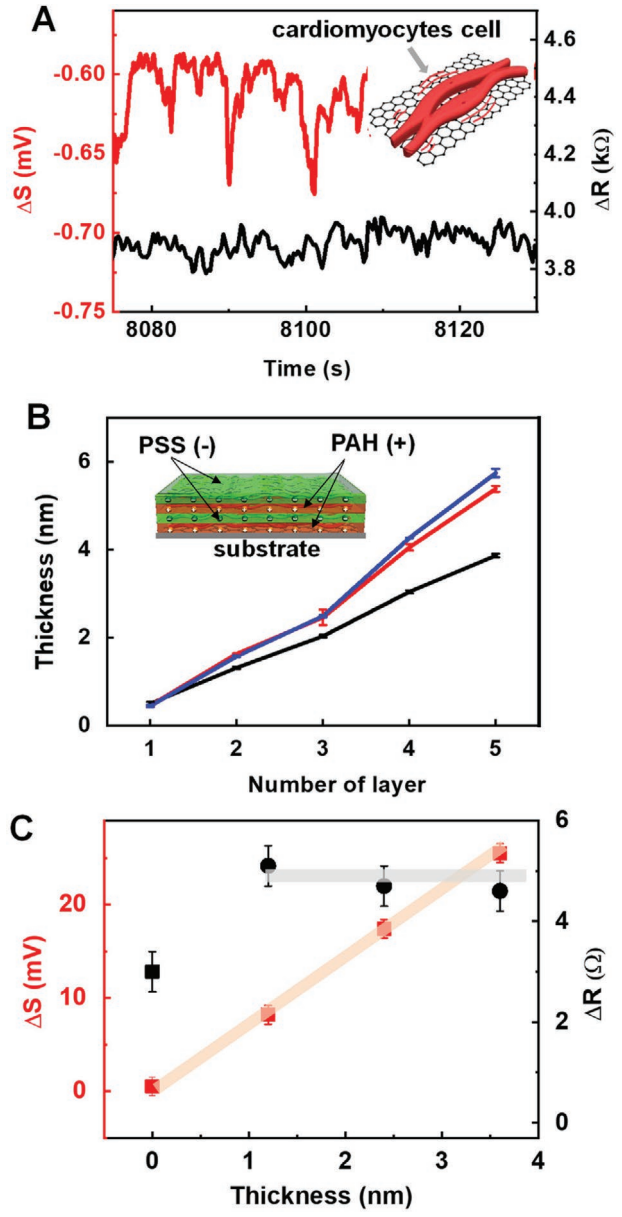

Figure 4. A) Detection of the unique contractility information of cardiomyocyte cell, which can be revealed by monitoring the dielectric-modulated UHF sensing signal but not the conventional Gr-FET sensing signal. Inset: Illustration of a cardiomyocyte cell on Gr-FETs. B) PEMs measured by ellipsometry. Three different salt concentrations (0.05, 0.5, and 1 M) were used, all with 10×10^{-3} M Trizma buffer. The bars indicate the range in which measured values are found. Inset is the scheme of LbL deposition of alternative PAH(+)/PSS(−). C) Both the direct current signal (ΔR, blue squares) and the UHF signal (S, red dots) are monitored and compared at the same time during the LbL deposition of PEMs.

engineered the sensing distance using polyelectrolytes, which are charged polymers and can be used to form polyelectrolyte multilayers (PEMs) with well-defined thicknesses using a layer-by-layer (LbL) deposition technique (Figure 4B, see the Experimental Section).[31,32] The as-fabricated PEMs have a thickness of ≈1.2 nm per layer in 1 M KCl on silicon wafer as characterized by ellipsometry measurements (Figure 4B). Interestingly, the introduction of the second PAH(+) was difficult to detect for the classical Gr-FET sensing as ΔR became flat (Figure 4C, black dots). In contrast, there was a clear change in the UHF signal ΔS which stems from the distinct dielectric properties of the substitute polyelectrolyte layer and the aqueous solution. We note here that we operated the UHF sensing at a liquid gate voltage where $\delta S/\delta V_{\mathrm{ref}} = 0$, so that we are able to ascribe the changes in the RF sensing signal to the capacitive variations close to the sensor surface. The robust distance dependence measurement above, further provides evidence that our UHF approach can probe biological solutions (i.e., up to about 4 nm away from the graphene surface beyond the Debye screening length of 0.3 nm in 1 M KCl solution[33]), where conventional field-effect sensors start to lose signal.

3. Conclusion

We have adopted high-quality single-crystal CVD graphene to develop graphene biosensors operated at UHF, where the conductivity of the water solution, and thus the ionic screening is fully cancelled and biochemical detection can be achieved with high sensitivities. Importantly, the electrolyte-gated UHF reflectometry detection scheme ensures the differentiation of the correlated sensing signals originated from either field-effect or dielectric-specified biomolecular/cell interactions/activities. These achievements highlight the unique potential of UHF operation to unlock the true potential of graphene biosensors, namely ionic screening in physiological conditions with high salt concentrations, for applications in POC detection.

4. Experimental Section

UHF Graphene Biosensor Assembly: A printed circuit board (PCB) was fabricated specifically for impedance matching based on a stub transmission line (TL) design,[16] and thus maximizing the RF biosensing signal (Figure S3A, Supporting Information). The graphene chip was mounted and wire bonded to the end of the TL. A transparent flow cell made of PMMA was then assembled on top of the graphene chip for liquid handling (Figure 1A, upper panel and Figure S3B, Supporting Information). This RF box was then connected to a home-made biological sensor setup (Figure S4, Supporting Information) for sampling both the UHF interferometry sensing signal S (in red) and the graphene resistance R (in blue) using a two-channel lock-in amplifier (Figure 1C). The conductance between the side gate electrode and the Red Rod reference electrode was monitored to make sure there is no air bubble in the microfluidic channel.

Reflectometry Measurements with Impedance Matching Circuit: The integrated UHF graphene biosensors were characterized by performing reflectometry measurements. The reflectometry consists detecting the reflected wave of a RF signal (or more specially measuring the reflection coefficient S11) depending on the load impedance. A 2 GHz stub-matching circuit on PCB was previously developed.[16] This can be applied as the matching network for sensitivity optimization by interfacing the characteristic 50 Ω impedance of RF measurement setups (the vector network analyzer, VNA) and the Gr-FET with typical resistance of 1–10 kΩ. The chosen frequency of 2 GHz was optimized for accurate biological detection, as biomolecules and water exhibit distinct contrast in permittivity and losses from electrolytes are preferentially small.[34]

Classic Resistance Measurement of Gr-FET: To recover the weak (and in our case slow) sensing signal, a lock-in amplifier (HF2LI, Zurich

Instruments) was used to measure the resistance measurement of Gr-FET with narrow bandpass filters (≈1 Hz). The HF2LI was used to generate a sinusoidal alternating voltage (with amplitude $V_{SD} \approx$ 10–100 mV) applied to the source and drain electrodes of the Gr-FETs, and the resultant source–drain current I_{SD} (resistance $R = V_{SD}/I_{SD}$) was monitored across the Gr-FETs (at a fixed liquid gate voltage V_{ref}) versus time using the ZiControl (Zurich Instruments) program. Therefore, when used for sensitive detection, the resistance change of the Gr-FETs can be monitored in real time with high accuracy.

High-Frequency-Operated Graphene Biosensor Measurement and Analysis: The design of the UHF graphene biosensor is based on an interferometric architecture with a signal path and a reference path. The signal from a UHF source (≈2 GHz and modulated at ≈kHz) was split between a sensing path and a reference path (LO). The sensing path contains a directional coupler connected to the graphene sensor through a bias tee, which enables simultaneous detection of the Gr-FET conductance at low frequencies. After amplification, the sensing signal were recombined with the LO using a mixer to form an UHF interferometer.

The UHF graphene biosensor was carefully operated around its resonant frequency (i.e., 1.83 GHz) to achieve optimal sensitivity and tune the phase difference between the paths (down to $S \approx 1$ mV as a tuning indicator) and relate it to the change in capacitance (Equation (1)). Adsorption of biomolecules on graphene surface replaces water dipoles and perturbs the field on the resonator leading to a phase shift detected in the output of the mixer. In the operational region, the difference in phase between the paths produces a small voltage signal that can be detected by the lock-in amplifier, which is in proportional to the change in capacitance ΔC[20]

$$S = G|V_{ref}||V_{res}|\left(\frac{\partial \varphi}{\partial C}\right)\Delta C \quad (1)$$

where G represents the gain of the mixer-and-lock-in amplifier. V_{ref} and V_{res} are the signals from the reference path and the sensing path, respectively. The rate of change in phase ϕ versus capacitance C can be estimated using

$$\frac{\partial \varphi}{\partial C} = -2Qf_0Z_0 \quad (2)$$

where f_0 is the resonance frequency and Z_0 is the characteristic impedance.

Peptide Synthesis, Functionalization, and Purification: Peptides E and K were synthesized using conventional solid-phase peptide synthesis techniques on a CEM Liberty Blue microwave-assisted peptide synthesizer. Upon completion of the peptide synthesis, a Fmoc-PEG_{12}-COOH linker (1.5 equivalents) was manually coupled to the N-terminus of peptide E using HCTU (1.5 equivalents) and DIPEA (1.5 equivalents). The linker was subsequently deprotected (20% piperidine in DMF) and 1-pyreneacetic acid (3 equivalents) coupled using HCTU (3 equivalents) and DIPEA (3 equivalents). The pyrene-functionalized peptide E and non-functionalized peptide K were cleaved from the resin using a mixture of TFA:water:TIPS (95:2.5:2.5%) and precipitated in ice-cold diethyl ether before being freeze-dried. The peptides were purified using high-pressure liquid chromatography (HPLC) and analyzed using mass spectrometry. Fractions that were deemed to be >95% pure were pooled and lyophilized.

Human Induced Pluripotency Stem Cell Culture and Differentiation into Cardiomyocytes: Human induced pluripotent stem cell line (hiPSC) LUMC0044iCTRL44.9 (L44) was obtained from Leiden University Medical Center (LUMC). hiPSCs were cultured on six-well plates coated with vitronectin in E8 medium (Stem Cell Technologies). Cells were passaged once per week with 0.5×10^{-3} M EDTA (Sigma-Aldrich). Specifically, on the passage day, cells were first washed with PBS and incubated with EDTA (0.5×10^{-3} M) for 5 min at 37 °C followed by 1 min at room temperature. After aspirating the EDTA solution, E8 medium with Revita Cell (1:200) (2 mL) was added to each well. A 2 mL pipet was used to flush and dissociate the cells (6–8 times). Cell pellets were obtained by centrifuge with 300 *g*, 5 min. After that, cells were replated and treated with E8 medium supplied Revita Cell (1:200) for 24 h and then refreshed with E8 medium every day prior to passage. The differentiation of hiPSCs were performed according to STEMdiff Cardiomyocyte Differentiation Kit (StemCell Technologies). Briefly, a 12-well plate coated with Matrigel (Corning) were first prepared according to protocol described in the paper.[35] On the passage day, hiPSCs were dissociated, counted, and replated as a density of 350 000 cells per well. Cells were treated with E8 medium supplied Revita Cell (1:200) for 24 h and then refreshed with E8 medium daily prior to differentiation. When the cell confluence reached 95%, cells were treated with differentiation medium from the STEMdiff Cardiomyocyte Differentiation Kit. On day 15, hiPSCs were fluorescently stained with calcein AM (2×10^{-6} M) and imaged using the EVOS FL AUTO2 equipped with a temperature controller and CO_2 gas. The spontaneous beating cardiomyocytes were recorded within a GFP fluorescence channel.

Reseeding of hiPSCs-Derived Cardiomyocytes on the Gr-FET Device: On Day 15, hiPSC-derived cardiomyocytes (hiPSC-CMs) were first dissociated by incubation with cardiomyocyte dissociation medium (StemCell Technologies) at 37 °C for 10–12 min. Then, the dissociated hiPSC-CMs were collected by centrifuge (300*g*, 5 min), counted and resuspended in cardiomyocyte support medium (StemCell Technologies). Finally, hiPSC-CMs were plated on GFET device with a density at 100 000 cells per device. The medium was refreshed daily until measurements were performed when the cells were observed to display spontaneous beating, which usually occurred after 7–8 days in vitro.

Multilayer Polyelectrolyte Deposition by LbL and Detection: During the LbL deposition, the graphene UHF device (negatively doped as it is fabricated on a negatively charged SiO_2/Si substrate) was first dipped in positively charged poly(allylamine hydrochloride) (PAH, +), followed by negatively charged poly(styrene sulfonate) (PSS, −), and PAH(+) again (in 1 M KCl and 10×10^{-3} M Tris solution, pH 8) allowing the controlled build-up of polyelectrolyte films[36] with well-defined thicknesses. The sequential PAH(+)/PSS(−) deposition process was monitored by detecting the reversal of the surface charges using either a conventional Gr-FET configuration or by detecting the changes in dielectric environment using UHF interferometry sensing.

Supporting Information

Supporting Information is available from the Wiley Online Library or from the author.

Acknowledgements

Financial support from the Basic Science Center Project of NSFC (No. 51788104), the National Natural Science Foundation of China (Nos. 52073160, 52173007), the National Key Research and Development Program of China (No. 2020YFF01014706), Swiss Science Foundation (SNSF P300P2-164663 and SNSF 364 P300P2_154557), European Commission Horizon 2020-Research and Innovation Framework Programme (Marie Sklodowska-Curie actions Individual Fellowship No. 749671), the European Research Council under the European Union's Seventh Framework Programme (FP/2007-2013)/ERC Grant Agreement No. 335879 project acronym "Biographene," and The Netherlands Organization for Scientific Research (NWO-VIDI 723.013.007 and NWO-VENI 722.014.004) is gratefully acknowledged.

Conflict of Interest

The authors declare no conflict of interest.

Data Availability Statement

The data that support the findings of this study are available from the corresponding author upon reasonable request.

Keywords

dielectric modulation, field effect, graphene biosensors, ionic screening, ultrahigh frequency

Received: August 24, 2021
Revised: October 26, 2021
Published online: January 6, 2022

[1] P. Bergveld, *IEEE. Trans. Biomed. Eng.* **1972**, *19*, 342.
[2] Y. Cui, Q. Q. Wei, H. K. Park, C. M. Lieber, *Science* **2001**, *293*, 1289.
[3] K. Besteman, J. O. Lee, F. G. M. Wiertz, H. A. Heering, C. Dekker, *Nano Lett.* **2003**, *3*, 727.
[4] C. Li, M. Curreli, H. Lin, B. Lei, F. N. Ishikawa, R. Datar, R. J. Cote, M. E. Thompson, C. W. Zhou, *J. Am. Chem. Soc.* **2005**, *127*, 12484.
[5] F. Schedin, A. K. Geim, S. V. Morozov, E. W. Hill, P. Blake, M. I. Katsnelson, K. S. Novoselov, *Nat. Mater.* **2007**, *6*, 652.
[6] E. Stern, J. F. Klemic, D. A. Routenberg, P. N. Wyrembak, D. B. Turner-Evans, A. D. Hamilton, D. A. LaVan, T. M. Fahmy, M. A. Reed, *Nature* **2007**, *445*, 519.
[7] H. Im, X. J. Huang, B. Gu, Y. K. Choi, *Nat. Nanotechnol.* **2007**, *2*, 430.
[8] P. Dwivedi, A. Kranti, *IEEE Sens. J.* **2018**, *18*, 3228.
[9] O. Knopfmacher, A. Tarasov, W. Fu, M. Wipf, B. Niesen, M. Calame, C. Schonenberger, *Nano Lett.* **2010**, *10*, 2268.
[10] A. Tarasov, W. Fu, O. Knopfmacher, J. Brunner, M. Calame, C. Schönenberger, *Appl. Phys. Lett.* **2011**, *98*, 012114.
[11] B. M. Lowe, K. Sun, I. Zeimpekis, C.-K. Skylaris, N. G. Green, *Analyst* **2017**, *142*, 4173.
[12] R. L. Stoop, M. Wipf, S. Müller, K. Bedner, I. A. Wright, C. J. Martin, E. C. Constable, W. Fu, A. Tarasov, M. Calame, C. Schönenberger, *Sens. Actuators, B* **2015**, *220*, 500.
[13] W. Fu, L. Jiang, E. P. van Geest, L. M. C. Lima, G. F. Schneider, *Adv. Mater.* **2017**, *29*, 1603610.
[14] L. Xu, D. Li, S. Ramadan, Y. Li, N. Klein, *Biosens. Bioelectron.* **2020**, *170*, 112673.
[15] G. S. Kulkarni, Z. H. Zhong, *Nano Lett.* **2012**, *12*, 719.
[16] W. Fu, M. El Abbassi, T. Hasler, M. Jung, M. Steinacher, M. Calame, C. Schönenberger, G. Puebla-Hellmann, S. Hellmüller, T. Ihn, A. Wallraff, *Appl. Phys. Lett.* **2014**, *104*, 013102.
[17] H. J. Lee, J. G. Yook, *Materials* **2019**, *12*, 952.
[18] T. H. Basey-Fisher, N. Guerra, C. Triulzi, A. Gregory, S. M. Hanham, M. M. Stevens, S. A. Maier, N. Klein, *Adv. Healthcare Mater.* **2014**, *3*, 536.
[19] Q. Chen, D. Roitman, A. Knoesen, *Sens. Actuators, A* **2009**, *152*, 151.
[20] M. Nikolic-Jaric, S. F. Romanuik, G. A. Ferrier, G. E. Bridges, M. Butler, K. Sunley, D. J. Thomson, M. R. Freeman, *Biomicrofluidics* **2009**, *3*, 034103.
[21] S. D. Sarma, S. Adam, E. H. Hwang, E. Rossi, *Rev. Mod. Phys.* **2011**, *83*, 407.
[22] J. R. Litowski, R. S. Hodges, *J. Biol. Chem.* **2002**, *277*, 37272.
[23] J. Yang, A. Bahreman, G. Daudey, J. Bussmann, R. C. Olsthoorn, A. Kros, *ACS Cent. Sci.* **2016**, *2*, 621.
[24] H. R. Marsden, N. A. Elbers, P. H. Bomans, N. A. Sommerdijk, A. Kros, *Angew. Chem., Int. Ed.* **2009**, *48*, 2330.
[25] H. R. Marsden, A. Kros, *Angew. Chem., Int. Ed.* **2010**, *49*, 2988.
[26] W. Fu, C. Nef, A. Tarasov, M. Wipf, R. Stoop, O. Knopfmacher, M. Weiss, M. Calame, C. Schonenberger, *Nanoscale* **2013**, *5*, 12104.
[27] U. Piran, W. J. Riordan, *J. Immunol. Methods* **1990**, *133*, 141.
[28] B. Park, H. G. Park, J. H. Ji, J. Cho, S. C. Jun, *Micromachines* **2016**, *7*, 136.
[29] L. H. Hess, M. Jansen, V. Maybeck, M. V. Hauf, M. Seifert, M. Stutzmann, I. D. Sharp, A. Offenhausser, J. A. Garrido, *Adv. Mater.* **2011**, *23*, 5045.
[30] M. Rabe, A. Boyle, H. R. Zope, F. Versluis, A. Kros, *Biopolymers* **2015**, *104*, 65.
[31] F. Wu, J. Li, Y. Su, J. Wang, W. Yang, N. Li, L. Chen, S. Chen, R. Chen, L. Bao, *Nano Lett.* **2016**, *16*, 5488.
[32] C. Jiang, C. Luo, X. Liu, L. Shao, Y. Dong, Y. Zhang, F. Shi, *ACS Appl. Mater. Interfaces* **2015**, *7*, 10920.
[33] E. Stern, R. Wagner, F. J. Sigworth, R. Breake, T. M. Fahmy, M. A. Reed, *Nano Lett.* **2007**, *7*, 3405.
[34] R. Pethig, *IEEE Trans. Dielectr. Electr. Insul.* **1984**, *19*, 453.
[35] E. Giacomelli, M. Bellin, V. V. Orlova, C. L. Mummery, *Curr. Protoc. Hum. Genet.* **2017**, *95*, 21901.
[36] J. M. C. Lourenco, P. A. Ribeiro, A. M. B. Do Rego, F. M. B. Fernandes, A. M. C. Moutinho, M. Raposo, *Langmuir* **2004**, *20*, 8103.